Estimation of the driving force for dioxygen formation in photosynthesis

Håkan Nilsson [a], Laurent Cournac [b,c], Fabrice Rappaport [d], Johannes Messinger [a,*], Jérôme Lavergne [e,*]

[a] Department of Chemistry, Kemiskt Biologiskt Centrum (KBC), Umeå University, Sweden
[b] Laboratoire de Bioénergétique et Biotechnologie des Bactéries et Microalgues (CEA/DSV/IBEB; UMR 6191 CNRS/CEA/Aix-Marseille Université), Saint-Paul-lez-Durance F-13108, France
[c] Institut de Recherche pour le Développement, Unité Mixte de Recherche Ecologie Fonctionnelle et Biogéochimie des Sols et Agro-Écosystèmes, F-34060 Montpellier, France
[d] Institut de Biologie Physico-Chimique, UMR 7141 CNRS and Université Pierre et Marie Curie, 13 rue Pierre et Marie Curie, 75005 Paris, France
[e] Laboratoire de Bioénergétique Cellulaire (CEA/DSV/IBEB; UMR 6191 CNRS/CEA/Aix-Marseille Université), Saint-Paul-lez-Durance F-13108, France

ARTICLE INFO

ABSTRACT

Photosynthetic water oxidation to molecular oxygen is carried out by photosystem II (PSII) over a reaction cycle involving four photochemical steps that drive the oxygen-evolving complex through five redox states S_i ($i = 0,\ldots, 4$). For understanding the catalytic strategy of biological water oxidation it is important to elucidate the energetic landscape of PSII and in particular that of the final $S_4 \to S_0$ transition. In this short-lived chemical step the four oxidizing equivalents accumulated in the preceding photochemical events are used up to form molecular oxygen, two protons are released and at least one substrate water molecule binds to the Mn_4CaO_5 cluster. In this study we probed the probability to form S_4 from S_0 and O_2 by incubating Y_D-less PSII in the S_0 state for 2–3 days in the presence of $^{18}O_2$ and $H_2^{16}O$. The absence of any measurable $^{16,18}O_2$ formation by water-exchange in the S_4 state suggests that the S_4 state is hardly ever populated. On the basis of a detailed analysis we determined that the equilibrium constant K of the $S_4 \to S_0$ transition is larger than 1.0×10^7 so that this step is highly exergonic. We argue that this finding is consistent with current knowledge of the energetics of the S_0 to S_4 reactions, and that the high exergonicity is required for the kinetic efficiency of PSII.

© 2015 The Authors. Published by Elsevier B.V. This is an open access article under the CC BY-NC-ND license (http://creativecommons.org/licenses/by-nc-nd/4.0/).

1. Introduction

Photosynthesis provides the chemical free energy and the molecular oxygen that most organisms on earth need for their survival. It also generated the organic matter that converted over geological time scales into the fossil fuels upon which most present human societies completely depend. Understanding the biological process of converting solar energy into chemical fuels, and how it can inspire artificial devices, may thus be of utmost importance [1].

Water is the source for photosynthetic oxygen production and for the electrons required for CO_2 assimilation. Its light-driven oxidation to molecular oxygen is powered by charge separations in the reaction center of photosystem II (PSII) that are induced by the absorption of visible light in the associated antenna complexes and subsequent excitation energy transfer [2–10]. The PSII reaction center comprises the photochemical electron donor P680, which is made of four chlorophyll-a molecules (Chl_{D1}, P_{D1}, P_{D2}, Chl_{D2}), and the primary electron acceptor molecule pheophytin (Pheo) (Fig. 1A). Absorption of visible light by the PSII-associated antenna and subsequent excitation energy transfer to the reaction center leads to the primary charge separation, i.e. to the formation of the radical pair $P_{680}^{\bullet+}Pheo^{\bullet-}$. The $P_{680}^{\bullet+}/P_{680}$ couple has an estimated oxidizing potential of about $+1200$ mV, the highest known in biology [11–14]. For minimizing harmful and wasteful charge recombination reactions, PSII has a set of electron redox-active cofactors that allow spatial and energetic separation of the radical pair [6] (Fig. 1A). The oxidized photochemical electron donor $P_{680}^{\bullet+}$ is reduced by a redox active tyrosine known as Y_Z, which is H-bonded to D1-His190 (Fig. 1B). Y_Z oxidation leads to the formation of the $Y_Z^{\bullet}His190^+$ pair by moving the proton within the H-bond [15,16]. This pair, that we denote Y_Z^{ox}, then oxidizes a chair-shaped cluster associating four manganese ions, one calcium ion and five bridging oxo-groups (Mn_4CaO_5 cluster) [17–21]. Four water-derived ligands bind to the cluster: two, W1 and W2, to the Mn-top of the 'chair', which is often referred to as the 'outer' Mn (or Mn_{A4}), and two, W3 and W4, to the Ca, which forms one corner of the cuboidal bottom of the chair. A Cl^- anion, not shown in Fig. 1, located about 7 Å away from Mn_{A4} [20,21] affects the turnover efficiency of PSII [22,23]. Together with its
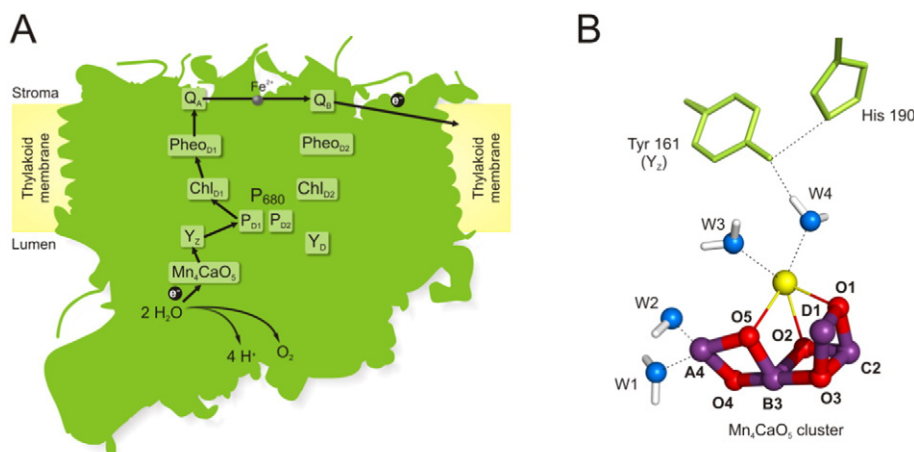
Fig. 1. Panel A shows the spatial organization of the redox cofactors in PSII and the electron transfer pathways between them. Panel B: Detailed view of the molecular structure of the Mn_4CaO_5 cluster in the S_1 state of PSII. In this orientation the 'chair' is lying side-wise. The figure is based on a crystal structure of a PSII monomer (PBD 3KZI) [32], while the geometry of the Mn_4CaO_5 cluster is based on density functional theory (DFT) calculations [33]. Mn ions: magenta (A4, B3, C2, D1), oxygen bridges: red (O1–O5), Ca ion: yellow, oxygen of water/hydroxo ligands: blue (W1–W4).

protein environment and surrounding water molecules this inorganic cluster forms the oxygen-evolving complex (OEC), which, after four successive oxidations by Y_Z^{ox}, oxidizes two water molecules to molecular oxygen. For recent reviews on PSII and its water oxidase, see e.g. [8,10,24–31].

The accumulation of oxidizing equivalents (holes) in the PS II electron donor chain is formally described by Kok's S-states model [34,35]. Each S_i state ($i = 0...4$) is characterized by the presence of i such equivalents, and each photochemical turnover promotes an increment of S_i to S_{i+1} until state S_4 is reached and the system spontaneously loops back to S_0 while dioxygen is released (Fig. 2). After sufficient dark-adaptation S_1 is the predominant state, since S_0, S_2 and S_3 revert by different pathways to S_1. Formation of the S_4 state triggers a series of reactions during which the four accumulated oxidizing equivalents are used up, the O–O bond is formed, molecular oxygen and two protons are released, and at least one substrate water molecule re-binds to the Mn_4CaO_5 cluster resetting it to the S_0 state. The Mn_4CaO_5 cluster is thus the crucial interface between the one-electron photochemistry in the reaction center, and the four-electron, four-proton chemistry involved for oxidizing two water molecules to molecular oxygen.

In this paper, we use the S_i notation for specifying the number (i) of oxidizing equivalents present in P_{680}, Y_Z and/or the Mn_4CaO_5 cluster (including substrate waters). This may – or may not – be the same as the number of equivalents ($j \leq i$) stored in the Mn_4CaO_5 cluster and we denote the state of the latter as M_j (as found in previous literature, e.g. Refs. [36,37]). Since the longest-lived form of state S_4 is in fact $P_{680}Y_Z^{ox}M_3$, this notation is less ambiguous than "$Y_Z^{ox}S_3$", which in current literature is variously referred to as an S_4 or S_3 state. There is as yet no experimental evidence for a state M_4 of the cluster, which may occur in the transition pathway to O–O formation. We also add information on the net charge present in the Mn_4CaO_5 cluster. As a first approximation (see [38–40]), one proton is released in the $S_0 \rightarrow S_1$ and $S_2 \rightarrow S_3$ transitions, and none on $S_1 \rightarrow S_2$, so that there is one net excess charge in states S_2 and S_3 compared to states S_0 and S_1 [25,41–43]. We shall keep track of this by featuring a '+' charge on the M system when appropriate (i.e., M_0, M_1, M_2^+, M_3^+). These notations are helpful for describing the successive forms of state S_4, where two protons are released at different stages (Fig. 2B).

The binding modes and sites of the substrate 'water' molecules to Mn_4CaO_5 cluster are not yet unambiguously identified. Rapid
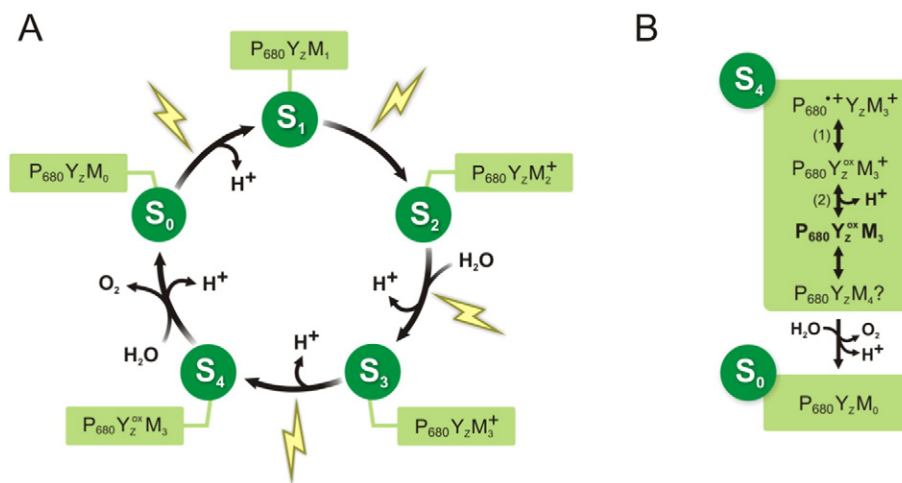
Fig. 2. Panel A shows the Kok cycle of water-oxidation to molecular oxygen by the OEC in PSII. Both the original S state nomenclature and the '$P_{680}Y_ZM$' notation used in this manuscript are given. B: $P_{680}Y_ZM$ notation of the sub-states discussed in this manuscript for the $S_4 \rightarrow S_0$ transition. $P_{680}Y_Z^{ox}M_3$ (in bold) is the most stable S_4 state intermediate, for which the equilibrium constant K is evaluated.

$H_2^{18}O/H_2^{16}O$ exchange experiments in combination with mass spectrometric detection of the isotopologues of O_2 produced by a set of µs flashes demonstrate that both substrate water molecules are exchangeable at different rates with bulk water molecules in all the S_i states. One of the two substrate water molecules is bound in all the S_i states to the Mn_4CaO_5 cluster, while the second substrate is bound at least in the S_2, S_3 and S_4 states [29,44,45]. Present evidence favors W2, W3 and/or O5 [29,31,45–49] (Fig. 1B) as substrate sites in the S_1 and S_2 states. An additional water, which likely becomes substrate in the next cycle [29,49,50], is reported to bind to the open coordination site on Mn_{D1} during the $S_2 \rightarrow S_3$ transition [19,50,51].

The driving force for O_2 formation in the $S_4 \rightarrow S_0$ transition has been a controversial issue for several years. In 2004 Clausen and Junge reported an experiment aimed at estimating this driving force by testing the effect of high oxygen pressure [52]. Increasing the concentration of the product will lower the equilibrium constant of the reaction, possibly bringing it to a stall if the effect is large enough. And such seemed to be the case, as the reaction was found half inhibited by only 2.3 bar O_2 partial pressure (i.e. ~10-fold the physiological oxygen concentration). This pointed to a rather small driving force (ΔG_0) of about 80 meV (i.e. an equilibrium constant $K \approx 20$) for this final step (expressed under normal atmospheric conditions), and suggested that PSII is operating close to reversibility. A far-reaching geochemical consequence was the possibility that the current oxygen concentration of the atmosphere was set by the energetic profile of the photosynthetic water oxidase. The finding of a low equilibrium constant was in line with an earlier study by Vos et al., using electroluminescence, where K was estimated to be about 65 [36].

However, the results of Clausen and Junge, which relied on the assignment of UV difference spectra to Mn oxidation state changes, were subsequently challenged by three independent studies. Haumann et al. employed time-resolved X-ray absorption measurements to follow the Mn oxidation changes directly during the turnover of PSII at O_2 pressures of up to 16 bar. These experiments revealed no blockage of the $S_4 \rightarrow S_0$ transition under any of the tested conditions [53]. Similarly, Kolling et al., using chlorophyll fluorescence to follow the S state turnover, found no evidence for product inhibition up to 11 bar O_2 [54]. Finally, some of us demonstrated by membrane-inlet mass spectrometry (MIMS) that the production of $^{18}O_2$ from $H_2^{18}O$ occurs at the same rate in the presence of 20 bar O_2 as with a similar N_2 pressure [55]. Thus, all three experiments point to a more substantial driving force than estimated by Vos et al. [36] and Clausen and Junge [52], but its exact magnitude remained unclear.

To estimate K, we designed a novel test for the $S_4 \leftrightarrow S_0$ equilibrium that is based on "Oxygen–Water Isotope Exchange" (OWIE) in the S_4 state. This was done using MIMS detection of the isotopic composition of the molecular oxygen after incubating PSII in the S_0 state in the presence of $^{18}O_2$ and $H_2^{16}O$. Thanks to the sensitivity of MIMS and to the long-term stability of the S_0 state in Y_D-less PSII preparations of *Thermosynechococcus elongatus* (*T. elongatus*) this method has unprecedented sensitivity. We report here a negative result that pushes the lower bound for K as high as 1.0×10^7. We argue that a high driving force for the $S_4 \rightarrow S_0$ reaction is consistent with the available knowledge on the energetics of the S states and with theoretical considerations on the relation between the ΔG_0 and the reaction rate.

2. Materials and methods

2.1. Sample preparation

WT and Y_D-less (D2-Y160F-PSII) mutants of *T. elongatus* were grown and PSII core complexes (PSIIcc) isolated as described previously [56]. After preparation all samples were frozen in liquid N_2 and stored at −80 °C until used.

For the experiments, the PSIIcc were suspended in a medium at pH 6.5 containing 15 mM $CaCl_2$, 15 mM $MgCl_2$, 40 mM MES and 1 M betaine (denoted as the "betaine buffer").

2.2. OWIE experiments

2.2.1. Partition of oxygen between aqueous and gas phases

The concentration of dissolved O_2 in water equilibrated with air at atmospheric pressure (i.e. a partial pressure of 0.21 bar) at T = 275 K is $[O_2]_0$ = 420 µM, corresponding to a coefficient of $K_{H,pc}$ = 498 L atm mol^{-1} in Henry's law (using Van't Hoff's equation with dln $K_{H,pc}$ / d(1/T) = 1500 K and $K_{H,pc}$ = 759 L atm mol^{-1} at 298 K [57]). From the ideal gas law, in a gas phase with volume V_G, and partial pressure P, one has N_G moles, with $N_G = P \times V_G / V_m$. After correcting for non-ideality [58], one gets V_m = 22.6 for T = 275 K and 1 atm. From Henry's law, in the liquid phase one has N_L moles such as $N_L = P \times V_L / 498$. Combining both expressions one gets:

$$N_G/N_L = 22.1 \, V_G/V_L \tag{1}$$

(independent of pressure). Hence, for equal gas and liquid volumes, ~95.5% of the oxygen molecules are present in the gas phase (at T = 298 K, the factor in Eq. (1) is 31.0 and the mole fraction in the gas phase is ~96.8%). Kinetic isotope effects for gas transfer into and out of water are in the per mil region and are thus neglected [59]. Two completely independent sets of OWIE experiments were performed to deal with the preference of O_2 to be in the gas phase. These are referred to in the following as OWIE-A and OWIE-B.

2.2.2. OWIE-A: gas phase sampling

Dark-adapted Y_D-less PSIIcc of *T. elongatus* (3 mg Chl/mL in betaine buffer pH 6.5) were synchronized in the S_0 state using the following illumination sequence: 1 laser pulse, 60 min dark, 3 pulses (spaced 1 s apart). The illumination and dark-incubation took place at room temperature in the absence of added electron acceptors using 200 µL aliquots in 4 mm diameter quartz EPR tubes. To achieve an even, saturating illumination the laser beam was divided into three beams of similar intensity that were aimed at the sample from three directions. The light source was a frequency-doubled Nd/YAG laser (Spectraphysics; 600 mJ/pulse; 9 ns pulse width). All subsequent steps were performed inside a glove box (VAC, Omni-Lab Systems) that maintained an inert N_2 atmosphere (~0.1 ppm O_2).

300 µL aliquots of the S_0-enriched PSII samples were loaded in the dark into septum capped vials (744 µL; V_G = 444 µL) and then purged with $^{18}O_2$ (Linde $^{18}O_2$, 97% enrichment) for 4 min under continuous stirring. The sample vials were sealed and incubated at 2 °C for up to 48.5 h under stirring. Five sample aliquots were withdrawn from the headspace (5 × 20 µL) at different times (0, 12.0, 24.0, 24.5 and 48.5 h) using a gas-tight sample lock syringe (Hamilton 1710SL). After sample withdrawal, the syringe needle was inserted through the small entry port into the MIMS sample chamber that was also placed inside the glove box. The needle was degassed for 15 min to remove the $^{18}O_2/N_2$ gas content in the needle (this process was monitored via the mass spectrometer). The headspace sample was subsequently injected into the reaction cell and the oxygen isotopologue concentrations were measured at m/z = 32, m/z = 34 and m/z = 36 from the peak amplitudes.

Control measurements were made with S_1Y_D-less PSIIcc (no preillumination) by incubating the dark-adapted sample with $^{18}O_2$. Three sample aliquots were withdrawn (3 × 20 µL) from the gas headspace at different time points (0, 12 and 24 h). The extent of gas leakage via the septum was determined by incubating water (300 µL) with $^{18}O_2$ and analyzing sample aliquots that were withdrawn from the gas headspace at 0, 23, 34 and 38 h.

The leakage of $^{18}O_2$ out of the vial was ~30% over 48 h, which was largely due to taking out a total of 80 µL from the gas phase for sampling (see Fig. S1 in the Supplementary Material). This leads to an average

concentration of $^{18}O_2$ in the aqueous phase of about 85% of its saturated value under 1 bar O_2 pressure ($\geq$97% $^{18}O_2$), i.e. $[^{18}O_2]$ = 1.65 mM.

The MIMS measurements were performed with a magnetic sector field isotope ratio mass spectrometer (ThermoFinnigan Delta V Plus) connected to the sample chamber (165 μL [44]) via a cooling trap filled with a dry ice/ethanol mixture [60–62]. The reaction cell was separated from the high vacuum inlet (5×10^{-8} bars) by a gas permeable silicon membrane, ~25 μm thickness (Mempro MEM-213) that was supported by a porous Teflon disk, ø $\approx$ 10 mm (Bel-Art Products).

2.2.3. OWIE-B: liquid sampling

Before enriching dark-adapted Y_D-less PSIIcc of *T. elongatus* in the S_0 state the sample suspension was saturated with $^{18}O_2$. Then, ~390 μL aliquots were filled into cylindrical glass tubes (length ~ 30 mm, internal diameter ~ 4 mm) and sealed with plasticine plugs, avoiding the presence of any significant gas space between the liquid and stopper. The Y_D-less PSIIcc suspensions had a Chl concentration of 270 μM in the betaine buffer at pH 6.5, with 100 μM phenyl-para benzoquinone (PPBQ) and 100 nM carbonylcyanide p-trifluoromethoxy-phenylhydrazone (FCCP). FCCP was added to the sample to accelerate the $S_2 \rightarrow S_1$ deactivation in order to reduce the time interval between the pre-flash and the group of three flashes to 60 s [63–65]. Control samples were prepared in the same way, but without PSII. The PSII samples were illuminated with laser pulses through a Y-shaped light guide with rectangular output windows, illuminating the tubes from both sides, thus ensuring saturating homogeneous illumination of the samples. After one pre-flash and 60 s darkness, three flashes spaced by 2 s were fired, setting PSII predominantly into the S_0 state. Half of the samples were tested right away and the other half was kept for three days in total darkness at 25 °C.

Both for the t = 0 and t = 72 h samples, the content of the tubes was divided into two parts: the first one (200 μL) was used for oxygen isotopes determination and the rest was 15-fold diluted, supplemented with 200 μM PPBQ as an electron acceptor and used for testing the O_2 evolution rate (measured by MS) under continuous light of saturating intensity. The determination by MIMS of the abundance of oxygen isotopes was carried out by laying down 200 μL of the samples on the inlet membrane under a nitrogen atmosphere. The response of the spectrometer to gas diffusion within the sample and across the membrane consisted of a ~15 s rise followed by a decrease ($t_{1/2} \sim 60$ s). For each isotope (m/z = 32, 34 and 36), we integrated the response over 60 s after the peak.

MIMS measurements were performed with a magnetic sector mass spectrometer (Thermo Fisher Scientific Prima-δB). The spectrometer was connected with a temperature-regulated sample chamber (cylindrical Hansatech oxygen electrode chamber) via a stainless steel vacuum line passing through a cooling trap consisting in a Dewar-held thermal bath fluid (Julabo Thermal HY) maintained at -80 °C by an immersion cooler (Julabo FT-902). The sample liquid phase was separated from the vacuum line by a 25 μm-thick Teflon membrane (YSI 5793) located at the bottom of the chamber and settled on a stainless steel frit disk. The measuring chamber was thermostated at 25 °C using a water jacket and continuously flushed with N_2 before and during sample deposition and analysis.

2.3. Determination of the S_0 population

The efficiency of the S_0 enrichment was tested with MS detection of flash-induced oxygen evolution patterns (FIOPs). Prior to the FIOP measurement the sample was diluted to a Chl concentration of 0.3 mg/mL in the betaine buffer pH 6.5 containing 0.5 mM PPBQ. Isotopically labeled water ($H_2^{18}O$, 97.6% enrichment, Medical Isotopes, Inc.) was added to the sample suspension (24% final concentration) to maximize labeled oxygen products. The sample was loaded into the mass spectrometer reaction cell and a series of 12 flashes (Xenon lamp, ~6 μs FWHM) spaced by 25 s dark periods were given to the sample to obtain the
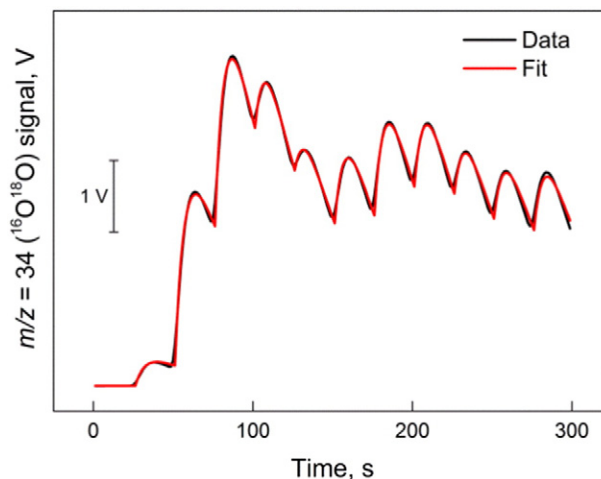

Fig. 3. FIOP of Y_D-less PSIIcc samples enriched in the S_0 state. The black curve is the experimental response of the MS (with $\Delta t = 25$ s between flashes) obtained with an $H_2^{18}O$-enrichment of 24%. The red curve is a fit with a 2-exponential function (Eq. S1 in Supplementary Material) to simulate the apparatus response and the following Kok parameters: miss coefficient = 15.8%, double hit coefficient = 5.14%, initial S_0 = 55% (and initial S_1 = 45%). An activity parameter of d = 0.96 was employed to account for the loss of active centers during the flash train. For details on the fit procedure see Text S1 with Figs. S2–S4 and Table S1 in Supplementary Material.

FIOP [44], as shown in Fig. 3. From a fit of these data, one estimates that the illumination procedure results in a 55% fraction of S_0 (for details see Text S1 with Figs. S2–S4 and Table S1 in the Supplementary Material).
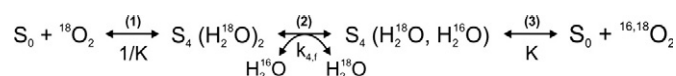
2.4. Long-term stability of S_0 in Y_D-less PSIIcc

To test the stability of the S_0 state over longer time periods, we monitored the EPR signal associated with S_0 [66,67] before and after 2-days dark-incubation on ice and even after 3-days at 20 °C. No significant change in the amplitude of the S_0 signal was observed, showing that no unwanted redox agent interacts with S_0 on a long time scale (see Text S2 with Fig. S5 in the Supplementary Material).

The overall resistance of the water oxidase to prolonged dark incubation at 25 °C was tested by measuring the oxygen evolution rate at the beginning and end (t = 72 h) of the incubation period. This showed an activity loss of ~5%.

3. Results

The Oxygen Water Isotope Exchange (OWIE) approach for determining the equilibrium constant K of the $S_4 \rightarrow S_0$ reaction relies on the exchange of one $H_2^{18}O$ substrate in state S_4 of photosystem II with one bulk $H_2^{16}O$ molecule (with a rate constant $k_{4,f}$ to be discussed later). Mass spectrometric detection of subsequent $^{16,18}O_2$ formation (or of $H_2^{18}O$) allows discerning if the S_4 state was transiently populated in the dark as a result of the equilibrium with S_0 and $^{18}O_2$ (Scheme 1):

$$S_0 + {}^{18}O_2 \underset{1/K}{\overset{(1)}{\rightleftharpoons}} S_4\,(H_2^{18}O)_2 \underset{\substack{\longleftarrow \\ H_2^{18}O}}{\overset{\substack{(2) \\ k_{4,f} \\ H_2^{16}O}}{\rightleftharpoons}} S_4\,(H_2^{18}O, H_2^{16}O) \underset{K}{\overset{(3)}{\rightleftharpoons}} S_0 + {}^{16,18}O_2$$

Reactions (1) and (3) are the equilibrium under study, with an associated constant of 1/K and K, respectively. Here, we denote as K the dimensionless ratio $[S_0] / [S_4]$, focusing on the pseudo first order $S_4 \leftrightarrow S_0$ reaction — assuming that the concentrations of the other reactants (water, oxygen, pH) are fixed at some standard state. The relation

of K with the midpoint potentials and concentrations of the reactants is examined in detail in the Discussion section.

The above scheme is simplified in several respects: proton binding/release reactions are not specifically considered and neither are equilibria between sub-states of S_4, which will be discussed later. Some production of $^{16}O_2$ may also occur from the exchange of both substrate water molecules, but this is a second order process that can be neglected.

The exchange of the substrate water molecules in state S_3 has been shown to occur with two different rate constants [29,44,68]. One water molecule "W_f" is exchanged in the tens of milliseconds range (in the present material, $k_{3,f} \approx 40$ s^{-1} at 20 °C and 19 s^{-1} at 10 °C [49,69]), whereas the other one, "W_s", is more tightly bound, with an exchange rate about 50-fold slower. In a recent study of water exchange in the S_4 state, using PSII with substituted cofactors (Sr^{2+} for Ca^{2+}; Br$^-$ or I$^-$ for Cl$^-$) in order to increase the lifetime of the S_4 state [45], it was shown that the exchange rates of both water-substrates are drastically slowed in state $P_{680}Y_Z^{ox}M_3$ as compared to $P_{680}Y_ZM_3^+$ (S_3). However, as argued in the Discussion section, the exchange cannot be totally blocked in the S_4 state, because of the equilibria between sub-states of S_4. Here we adopt the conservative assumption under which the substrate water exchange properties in state $P_{680}^{\bullet+}Y_ZM_3^+$ (belonging to the S_4 set) are unmodified with respect to the $P_{680}Y_ZM_3^+$ (S_3) state (Fig. 2). In this case, the exchange rates in S_4 should be slowed (with respect to S_3) by a factor that cannot exceed the equilibrium constant $K_{PZ} = [P_{680}Y_Z^{ox}M_3] / [P_{680}^{\bullet+}Y_ZM_3^+]$, i.e. about 130 (see Discussion section). The exchange rate denoted $k_{4,f}$ is thus $\geq k_{3,f}/K_{PZ}$.

On that basis, we now establish the equation for the OWIE production of $^{16,18}O_2$ when incubating PSII-enriched in state S_0 (denoting the concentration as $[S_0]$) for a time lapse t. Since $k_{4,f}$ is much slower than the equilibration rate in equilibrium (1) — which is about 1000 s^{-1} [70–76] — the concentration of $S_4(H_2^{18}O)_2$ remains constant and close to its equilibrium value; since the same is true for equilibrium (3), basically all $S_4(H_2^{18}O;H_2^{16}O)$ that is formed in reaction (2) will give rise to $^{16,18}O_2$ formation. We also make the assumption (experimentally substantiated below) that the OWIE process causes a negligible relative depletion of $^{18}O_2$; similarly, $[S_0]$ remains constant since it is returned by reaction (3). With these simplifications we obtain a 'steady-state approximation' with a pseudo-zero order rate equation for $^{16,18}O_2$ formation:

$$\left[{}^{16,18}O_2\right]_{OWIE} = t \times k_{4,f} \times \left[S_4\left(H_2{}^{18}O\right)_2\right] \qquad (2)$$

$$= \frac{t \times k_{4,f} \times [S_0] \times \left[{}^{18}O_2\right]}{[O_2]_0} \times \frac{1}{K} = \frac{X}{K}.$$

$[{}^{16,18}O_2]_{OWIE}$ is the concentration of $^{16,18}O_2$ produced by the OWIE process; $[{}^{18}O_2]$ is the concentration of dissolved $^{18}O_2$ and $[O_2]_0$ is the standard concentration of O_2 ($[O_2]_0 = 276$ μM; solubility of O_2 in water at 298 K in 1 atm air); thus $[S_4(H_2^{18}O)_2]$ equals $[S_0]$ / $K \times [{}^{18}O_2] / [O_2]_0$ at the applied partial oxygen pressure. X is a shorthand notation for the first factor in Eq. (2): it is the OWIE production that would correspond to the same amount of PSII maintained in the S_4 state. Recently reported negative clustering effects for ^{18}O-isotopes are in the −0.4‰ range for photosynthetic water oxidation [77] and thus without consequence for our experiments.

For this method to be a sensitive probe for the equilibrium constant K one needs PSII centers that do not inactivate and maintain a high S_0 population during extended periods (2–3 days) of dark-incubation with $^{18}O_2$ at physiological temperatures. PSII centers are known to be predominantly in the S_1 state after dark-adaptation. This has been explained by the reduction of S_2 and S_3 back to S_1, and the slow ($t_{1/2} = 10$–70 min at 20 °C in *T. elongatus* thylakoids [56,78,79]) oxidation of S_0 to S_1 by the oxidized auxiliary tyrosine Y_D (Y_D^{ox}), which is generally in its oxidized form after illumination. To stabilize S_0 over long

periods of time one needs to either chemically reduce Y_D^{ox}, or replace Y_D with a redox inert amino acid by mutation. Since a Y_D-less mutant was available (D2-Y160F-PSII) for *T. elongatus* [56], we employed this sample for the OWIE experiments. Test measurements showed (see Sections 2.3 and 2.4) that the rate of oxygen evolution of the Y_D-less PSIIcc preparation dropped only by 5% during a 72 h incubation at 25 °C, and that our flash–illumination sequence employed prior to the OWIE experiments produced S_0-enriched Y_D-less PSIIcc with an S state distribution of 55% S_0 and 45% S_1. EPR measurements confirmed that this S_0 population is stable at 20 °C for 48–72 h (see Text S2 with Fig. S5 in the Supplementary Material).

One additional technical challenge is that according to Henry's law the concentration of oxygen in water is only a small fraction of that in the gas phase above (see Section 2.2.1). We ran two series of experiments to cope with this. In the OWIE-A approach a gas phase was present in the incubation vials and a gas aliquot, kept small enough to keep the gas pressure above the liquid phase nearly unchanged, was taken and introduced into the mass spectrometer to probe for a change in the $^{16,18}O_2/{}^{18}O_2$ ratio, while in the OWIE-B approach the samples were devoid of a significant gas phase within plasticine-plugged tubes and an aqueous aliquot was used for MIMS detection of the O_2 isotopologues.

OWIE-A. Fig. 4 summarizes the results of the OWIE-A experiment in which the S_0-enriched Y_D-less PSIIcc were incubated in the dark at 2 °C for up to 48 h in the presence of $^{18}O_2$ within septum-sealed glass vials. As controls, S_1 samples and buffer samples were exposed to the same treatment. The data in Fig. 4 display the $^{16,18}O_2/{}^{18}O_2$ ratio as a function of incubation time for the three sample types. In case of a $^{16,18}O_2$ production via the OWIE effect one expects that this ratio (blue squares in Fig. 4) increases with time above those of the two controls (black circles and triangles in Fig. 4; this was not observed within the accuracy of the experiments. In order to obtain a lower estimate for K, this finding is analyzed more quantitatively below.

From the experimental scatter we estimate the standard deviation in the determination of the $^{16,18}O_2/{}^{18}O$ ratio to $\sigma = 3.8 \times 10^{-4}$. Fig. 4 shows that all data points were found within the $\pm 2\sigma$ interval (dashed horizontal lines) with respect to the average value, which corresponds to the $^{16,18}O_2$ content of the $^{18}O_2$-enriched gas used during incubation (solid line). With this 2 σ threshold, the smallest deviation of the $^{16,18}O_2/{}^{18}O_2$ ratio that we should be able to resolve was thus about 7.5×10^{-4}. To convert this into a threshold for OWIE production detection expressed as a concentration, we multiply this value by the average $^{18}O_2$ concentration in the gas phase ($1/22.6$ M $\times 0.97 \times 0.85$)

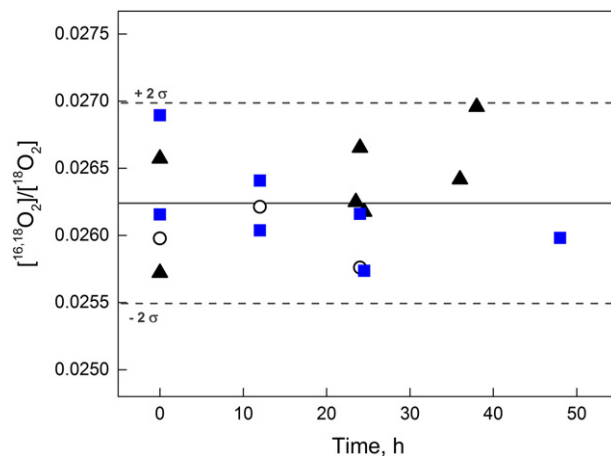**Fig. 4.** $^{16,18}O_2/{}^{18}O_2$ isotopologue ratio of the $^{18}O_2$-enriched gas phase in septum-sealed vials as a function of incubation time (hours) in presence of either Y_D-less PSIIcc enriched in the S_0 state (squares) or S_1-state (circles), or of water (triangles). For experimental details see Section 2.2.2 (OWIE-A).

Table 1
Summary of OWIE results.

	t (s)	$[S_0]$ (μM)	$[^{18}O_2]$ (μM)	$k_{4,f}$ (s^{-1})	X (μM)	$[^{16,18}O_2]_{OWIE}$ (μM)	K
OWIE-A	172,800	53.2	1650	0.077 s^{-1}	4.2×10^6	≤ 28.1	$\geq 1.5 \times 10^5$
OWIE-B	259,200	4.3	716	0.440 s^{-1}	1.3×10^6	≤ 0.12	$\geq 1.0 \times 10^7$

$k_{4,f}$ is $k_{3,f}$ / 130 as explained in the text, with $k_{3,f}$ = 10 s^{-1} at 2 °C (OWIE-A) or 57 s^{-1} at 25 °C (OWIE-B), as extrapolated from an Arrhenius plot from data at 20 °C and 10 °C [45,69]. X (see Eq. (2)) is the product of the four preceding columns divided by the reference oxygen concentration $[O_2]_0$ = 276 μM. The value of $[S_0]$ corresponds to 0.55 × [PSIIcc], with [PSIIcc] estimated from the chlorophyll concentration assuming 35 Chl/PSII. The average $^{18}O_2$ concentration takes into account the solubility of O_2 in water at the experimental temperature, the enrichment of the $^{18}O_2$ gas employed and the leakage of $^{18}O_2$ out of the vial during incubation. For details see Section 2.2.

and get a figure of 27.4 μM $^{16,18}O_2$. Since at the employed N_G/N_L ratio and T = 275 K only 3.1% of the O_2 is dissolved in the buffer (Eq. (1) and Section 2.2.2), the detectable $^{16,18}O_2$ production is only marginally larger than that, $[^{16,18}O_2]_{OWIE} \leq 28.1$ μM.

On the basis of the parameters summarized in Table 1, the value of X in Eq. (2) can be computed as X = 4.2×10^6 μM. Taking into account the above derived upper limit for $[^{16,18}O_2]_{OWIE}$, we obtain, using Eq. (2), a first lower limit for the equilibrium constant: K ≥ 1.5×10^5.

OWIE-B. Fig. 5 summarizes the results of the OWIE-B experiment, in which we tried to avoid any gas phase about the PSII suspension and assayed directly the liquid phase by isotope ratio MIMS. Since for this experiment all $^{16,18}O_2$ contained in the $^{18}O_2$-enriched gas and from incoming air was mathematically subtracted (see below), any $^{16,18}O_2$ production should lead to a positive deviation from the zero line of the $^{16,18}O_2/^{18}O_2$ ratio. This is obviously not the case since the blue symbols (D, E) signifying the $^{16,18}O_2/^{18}O_2$ ratio obtained with the 'best' S_0-enriched Y_D-less PSIIcc samples fall right into the 2σ uncertainty range of the experiment.

For these experiments seven tubes containing Y_D-less PSIIcc in $^{18}O_2$-enriched medium were prepared and submitted to pre-illuminations for S_0 enrichment. Seven control tubes containing no PSII were prepared in the same way. Two samples of each sort were tested right away by MIMS ("t = 0", in fact within a couple of hours) and the remaining 2 × 5 samples were tested after 72 h incubation in the dark at 25 °C. The main difficulty in this procedure is achieving bubble-free, well-sealed samples. The plasticine plugs

Fig. 5. Data from a OWIE-B experiment involving a 72 h incubation. The horizontal scale is the $[^{16}O_2]/[^{18}O_2]$ ratio measured on each sample. This increases during the incubation period due to imperfect tightness of the tubes. The vertical scale is the $[^{16,18}O_2]/[^{18}O_2]$ ratio of each sample, corrected by subtracting a base line: a × $[^{16}O_2]/[^{18}O_2]$ + b (with a = 0.0396 and b = 4.54×10^{-3}), which takes into account the isotopic compositions of the oxygen from the air and from the gas used for $^{18}O_2$-enrichment. In the absence of any additional isotopic conversion (such as the OWIE process), the data points should be close to zero within experimental accuracy (e.g., between the ±2 σ lines shown in the figure). The data points are featured as letters: A (two points), controls without PSIIcc and short incubation time (t = 0 h). B, controls without PSIIcc, incubated for t = 72 h. C, samples with S_0-enriched PSIIcc at t = 0 h. D, E, samples with S_0-enriched PSIIcc at t = 72 h. Sample E is the "best" sample with less air contamination (smaller $[^{16}O_2]/[^{18}O_2]$) than D. The standard deviation σ was computed from points A, B, C (8 samples).

were in fact more or less leaky, resulting in a progressive loss of $^{18}O_2$ of variable extent. Three PSII samples had to be rejected: two were too leaky and had reached complete equilibrium with air at t = 72 h and one tube was rejected because of a sizeable bubble, in which most of the putative OWIE-produced $^{16,18}O_2$ would have partitioned. In the two remaining tubes (points D and E in Fig. 5), the $^{18}O_2$ concentration was still relatively high and its value was used to estimate the average $^{18,18}O_2$ concentration during the incubation, assuming exponential decay. The initial value required in this computation was taken as the average from the t = 0 samples (1.38 mM – this is slightly above the equilibrium concentration predicted by Henry's law, due to using a cool medium and overpressure when preparing the sample). In this experimental round and in preliminary tests, we obtained little scatter in the measurements run at t = 0, because the imperfect plug tightness is inconsequential at short times. In the "best" sample (i.e. with minimal leakage, point E), the final amount of $^{18}O_2$ was 310 μM and the computed average $[^{18}O_2]$ = 716 μM. This value and other parameters involved in Eq. (2) are featured in Table 1, leading to X ≈ 1.3×10^6 μM.

Based on the control samples and also using the t = 0 PSIIcc samples, we can compute the standard deviation for the determination of the $^{16,18}O_2/^{18}O_2$ ratio: $\sigma = 1.9 \times 10^{-4}$. Clearly, the results obtained for the two PSII samples at t = 72 h (points D and E in Fig. 4) give $^{16,18}O_2/^{18}O_2$ ratios that are within the ±2 σ interval: we thus have again a negative result showing that the actual OWIE production must have been below the detection threshold. Considering the best sample in which the final amount of $^{18}O_2$ was 0.31 mM (point E), and assuming a 2 σ discrimination, we estimate that the detection threshold of $^{16,18}O_2$ in this experiment was 0.12 μM. Thus, we conclude that $[^{16,18}O_2]_{OWIE} \leq 0.12$ μM, which implies that, with the above value of X, K ≥ 1.0×10^7.

4. Discussion

4.1. OWIE experiments

According to current knowledge, the S_4 state encompasses at least three detectable sub-states as featured in Fig. 2B. Reaction (1) is the electron transfer from tyrosine Y_Z to $P_{680}^{\bullet+}$, taking place in the 100 ns time range [80–82]. Reaction (2) is a proton release step occurring in the 100 μs time range [83–88]. The thereby formed state, $P_{680}Y_Z^{ox}M_3$, is the longest-lived one, with a lifetime of about 1 ms. Its decay is accompanied by the release of O_2 and of the last proton and re-formation of S_0 without a resolvable intermediate; it thus corresponds to the rate-limiting reaction in the water oxidation process [84,89–92].

The free energy gap between $P_{680}^{\bullet+}/P_{680}$ and Y_Z^{ox}/Y_Z, in the presence of M^+, is probably about 13 meV (see [5,13], Supplementary Material Text S3 and references therein). Furthermore, according to Refs. [25,84], one may expect a $pK_a \approx 4.6$ (in the presence of Y_Z^{ox}) for the group which releases a proton on step (2). This is inferred from pH titrations showing inhibition of the $S_4 \rightarrow S_0$ transition around pH = 4.6, which corresponds to a free energy difference of 59 meV × (pH − pK_a) = 112 meV at pH 6.5 for the H^+ releasing step. This implies an overall free energy gap of ≈ 125 meV between states $P_{680}^{\bullet+}Y_ZM_3^+$ and $P_{680}Y_Z^{ox}M_3$ and thus an equilibrium constant $K_{PZ} \approx 130$. In the recent study of substrate-water exchange in the S_4 state [45] a slowing of the exchange rate of
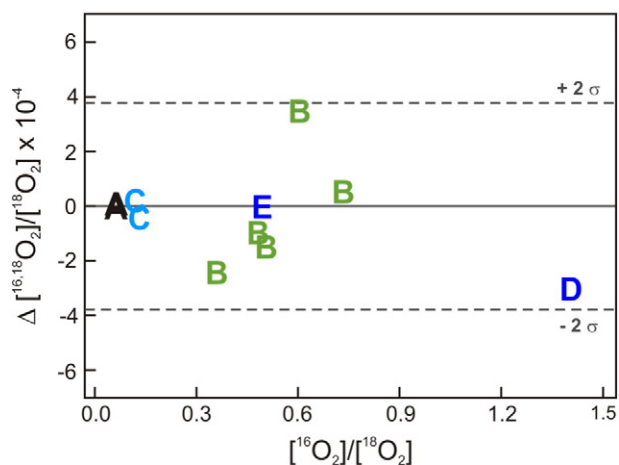
both substrates in S_4 by a factor of at least 100 with respect to S_3 state was observed. Several possibilities were considered as to the origin of the 'blocked' exchange in S_4. In one of these, the blocking is a result of the deprotonation step (2) in Fig. 2 B. This would imply a ≈ 100-fold slowing of the exchange rates (the equilibrium constant of step 2). In other interpretations the exchange is already blocked in state $P_{680}Y_Z^{ox}M_3^+$ due either to a rearrangement of the H-bond network caused by Y_Z oxidation, or to a possible requirement for an uphill reduction of Mn^{IV} by (reduced) Y_Z [45,93]. In such cases, the only sub-state of S_4 where water exchange occurs at the same rate as in S_3 would be state $P_{680}^{\bullet+}Y_ZM_3^+$ and the effective exchange rates observed in S_4 would be slowed by $K_{PZ} ≈ 130$ with respect to S_3. This conservative hypothesis was adopted here, giving $k_{4,f} = k_{3,f}/130$.

According to the OWIE-B experiments (Table 1), the lower bound for K is $≈ 1.0 × 10^7$ and thus $\Delta G_0(S_4 → S_0)_{OWIE} ≥ 410$ meV. We thus conclude that the $S_4 → S_0$ reaction is highly exergonic, much above the range that is presently accessible to investigations using high oxygen pressure. In the following, we argue that such a high equilibrium constant should not appear as a surprise: it could actually be expected from both experimental and theoretical knowledge.

4.2. The S_0/S_4 equilibrium constant seen from the photo-oxidation side

4.2.1. Equation for the equilibrium constant K

In this section we recall the relation of K with the midpoint potential of the reactants and their concentration (pH, $[O_2]$). The redox equilibrium between the O_2/H_2O and S_4/S_0 couples implies:

$$E_{O2} + \frac{RT}{4F} \ln \frac{[O_2][H^+]^4}{[H_2O]^2} = E_{40} + \frac{RT}{4F} \ln \frac{[S_4][H^+]^n}{[S_0]} \quad (3)$$

R is the gas constant, T the absolute temperature, F the Faraday constant; E_{O2} and E_{40} are standard potentials for the O_2/H_2O and S_4/S_0 couples, respectively. The factor 4 accounts for the fact that we are dealing with 4-electron reactions. The exponent n for $[H^+]$ in the right hand side denotes the number of protons that are released when going from S_0 to S_4 (through the photochemical pathway). This is related to the number of protons m released during the $S_4 → S_0 + O_2 + m\,H^+$ process (m = 4 − n), i.e. the difference between the 4 protons released by water oxidation and the n protons re-bound by the enzyme in S_0. For defining E_{40} and n, it is important to specify which S_4 sub-state is actually considered. From the photochemical formation of S_4 (state $P_{680}^{\bullet+}Y_ZM_3^+$) to its relaxation to S_0, 1.5–2 protons are released (with little pH dependence in the pH 6–7.5 range) [38–40], while 2–2.5 protons are released at earlier steps of the Kok's cycle. Incidentally, a non-integer value is not aberrant: it would just mean that some centers release one net proton and some release none, due to the pK_a's of the groups involved in the process, which includes the deprotonation of water and proton binding to the S_0 state of the enzyme. For simplicity, we have adopted in this paper a round figure of 2 protons released in the overall S_4 to S_0 process. As illustrated in Fig. 2, their release occurs in two steps, a rapid (~ 100 μs) release of 1 H^+, associated with the formation of $P_{680}Y_Z^{ox}M_3$, and a slower release accompanying the ~ 1 ms transition to S_0 [83–86]. So, if we adopt the convention that Eq. (3) applies to state $P_{680}Y_Z^{ox}M_3$ (the longest lived member of the S_4 family), one has $m ≈ 1$ and the standard potential E_{40} is understood in reference to that state.

As to the other specifications of standard conditions in Eq. (4), we adopt T = 298 K, pH = 7 and $[O_2]$ = 276 μM and $[H_2O]$ = 56 M. The value of E_{O2} under such conditions is 805 mV. By normalizing the reactants to these standard conditions and converting to decimal log, one obtains after rearranging Eq. (3):

$$\log K ≡ \log\left(\frac{[S_0]}{[S_4]}\right)_{eq} = \frac{E_{40} - 805}{15} + pH - 7 - \log\frac{p_{O2}}{0.21}. \quad (4)$$

Here, p_{O2} stands for the partial pressure of O_2 in atm and the release of m = 1 proton is assumed. The factor 15 is the rounded numerical value of $\ln(10) × RT / 4F = 14.78$ mV at 298 K.

4.2.2. Information from previous work about the potential E_{40} of the S_4/S_0 redox couple

In the various approaches mentioned thus far, the focus has been on the $S_4 → S_0$ reaction. But, since we are dealing with a cycle, estimates for E_{40} or K can also be obtained by considering the sequence of $S_0 → S_1 → ... → S_4$ reactions, which create four holes at the mean potential E_{40} [25,37]. In each of these four light-driven steps the energy gained by the system corresponds to that delivered by $P_{680}^{\bullet+}$ minus the loss involved in stabilizing the positive hole on its final location. Thus, the potential of the S_i/S_{i-1} couple is equal to the potential of the $P_{680}^{\bullet+}/P_{680}$ couple, E_P, minus a potential drop which corresponds to the free energy change occurring during the $P_{680}^{\bullet+}Y_ZM_{j-1} → P_{680}Y_ZM_j$ reaction, which we note $\Delta G_0(S_i)$. One should take into account, however, the fact that the midpoint potential of P_{680} is sensitive to the presence of the additional positive charge of the Mn_4CaO_5 cluster in the S_2 and S_3 states (i.e. the M_2^+ and M_3^+ states featured in Fig. 2A). We denote by E_P and E_P^+ the potential of P_{680} in the absence or presence of the additional charge, respectively. Evidence for this effect appears in the kinetics of $P_{680}^{\bullet+}$ reduction and as an electrochromic shift of the P_{680} absorption spectrum. The analysis of these effects in Text S3 of the Supplemental Material allows a rough estimate of the potential shift $E_P^+ - E_P ≈ 50$ mV. Therefore, the total energy accumulated is (in eV units) 2 E_P + 2 E_P^+ minus the sum of the $\Delta G_0(S_i)$ (with $i = 1...4$). These free energy drops have been estimated in previous work, as compiled below:

(i) $\Delta G_0(S_2)$: on the basis of recombination rates this was estimated at ~ 240 meV (see the Discussion section and Refs. [11,13])

(ii) From the ~ 15 °C lower temperature of the thermoluminescence band associated with the $S_3Q_A^-$ recombination as compared to $S_2Q_A^-$ [94,95] one infers [96] a $\Delta G_0(S_3)$ that is smaller by ~ 40 meV than $\Delta G_0(S_2)$; thus $\Delta G_0(S_3)$ ~ 200 meV

(iii) As mentioned above (Section 4.1), the free energy gap between $P_{680}^{\bullet+}/P_{680}$ and Y_Z^{ox}/Y_Z is (in the presence of the M^+ charge) about 13 meV (in the stabilized state reached after a few μs) [13]. Adding the 112 meV further stabilization due to proton release in the $P_{680}Y_Z^{ox}M_3^+ → P_{680}Y_Z^{ox}M_3$ step (Fig. 2), one obtains (for state $P_{680}Y_Z^{ox}M_3$): $\Delta G_0(S_4)$ ~ 125 meV.

(iv) According to Vass and Styring the potential difference between the S_2/S_1 and S_1/S_0 couples is ~ 210 meV [97]. We adopt $\Delta G_0(S_1) ≈ 240 + 210 = 450$ meV.

These values are summarized in Fig. 6. The average stabilization in the four steps (i–iv) is thus ≈ 255 meV, and $E_{40} = E_{P'} - 255$ mV, where $E_{P'} = (E_P + E_P^+) / 2$. The midpoint potential of $P_{680}^{\bullet+}/P_{680}$, in absence of an extra positive charge on the Mn_4CaO_5 cluster, has been estimated at $E_P = +1265$ mV or $E_P = +1170$–1210 mV [11,14]. Adopting the range 1170–1265 mV for E_P, and accordingly 1220–1315 mV for E_P^+, one obtains E_{40} in the range + 940 mV to + 1035 mV. The gap between these values is here entirely due to the uncertainty on E_P, but uncertainties on some other ingredients are important as well so that the "error bar" may still be larger. When inserted into Eq. (4) (with pH = 7, p_{O2} = 0.21 atm and T = 298 K), these values locate K in a range of 10^9–10^{15}. The 100 mV "uncertainty" for midpoint potential results in a very large range for K, because we are dealing with a four-electron reaction. In this respect, the impact of having n = 4 in the RT/nF factor may have been overlooked in previous literature: a moderate potential difference $E_{40} - E_{O2} = 100$ mV, for instance corresponds to an equilibrium constant ~ 10^7, because the "driving force" is in fact 4 × 100 meV.

Prior to the high pressure experiments starting with the work by Clausen and Junge [52], a first estimation of K was reported by Vos
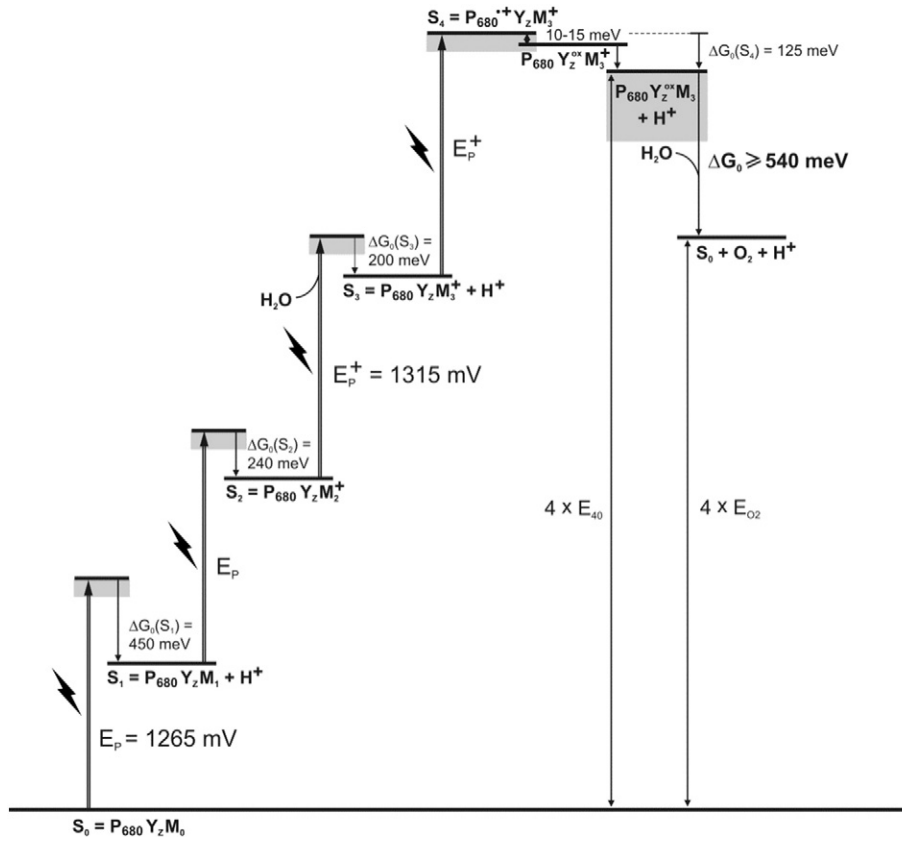
Diagram labels:
- $S_4 = P_{680}^{\bullet+}Y_ZM_3^+$
- 10-15 meV
- $P_{680}Y_Z^{ox}M_3^+$
- $\Delta G_0(S_4) = 125$ meV
- $P_{680}Y_Z^{ox}M_3 + H^+$
- E_P^+
- H_2O $\Delta G_0 \geqslant 540$ meV
- $\Delta G_0(S_3) = 200$ meV
- $S_0 + O_2 + H^+$
- H_2O
- $S_3 = P_{680}Y_ZM_3^+ + H^+$
- $E_P^+ = 1315$ mV
- $\Delta G_0(S_2) = 240$ meV
- $S_2 = P_{680}Y_ZM_2^+$
- $4 \times E_{40}$ $4 \times E_{O2}$
- E_P
- $\Delta G_0(S_1) = 450$ meV
- $S_1 = P_{680}Y_ZM_1 + H^+$
- $E_P = 1265$ mV
- $S_0 = P_{680}Y_ZM_0$

Fig. 6. Diagram visualizing the stepwise energy gain due to successive photon absorption by PSII. The energy difference between the initial S_0 and final S_0 states is stored in the bonds of the oxygen molecule formed by water splitting at the Mn_4CaO_5 cluster and by the entropic contributions discussed in Section 4.3. E_P is the potential of $P_{680}^{\bullet+}/P_{680}$ in presence of M (S_0 and S_1 states), while E_P^+ is the potential for the same redox couple in presence of M^+ (S_2 and S_3 states). This difference can be estimated to be ≈ 50 mV (see Text S3 in Supplementary Material). The maximal current literature estimate of $E_P = 1265$ mV was adopted for this Figure, and the range to the lower recent literature estimate for $E_P = 1170$ mV is indicated by gray bars [11,14]. The lower edge of the gray bar for the energy level of the S_4 reference state $P_{680}Y_Z^{ox}M_3$ results from adopting the lower estimate for E_P/E_P^+ in the preceding charge separations. E_{O2} and E_{40} are the standard potentials for the O_2/H_2O and S_4/S_0 couples, respectively. The potential drops occurring after the light absorptions correspond to the free energy changes occurring during the $P_{680}^{\bullet+}Y_ZM_{j-1} \rightarrow P_{680}Y_ZM_j$ reactions, which we denote $\Delta G_0(S_i)$.

et al. from an electroluminescence study [36]. The equilibrium constant for the $P_{680}Y_Z^{ox}M_3 \rightarrow P_{680}Y_Z S_0 (O_2)$ reaction was estimated at $K \approx 65$ (or $\Delta G_0 \approx 105$ meV; as emphasized above this would mean that E_{40} lies only $105/4 = 26$ mV above E_{O2}). This was derived from the decay of the amplitude of the electroluminescence spike when varying the delay between the (third) flash and the voltage pulse used as a probe. The information concerns the 1.2 ms phase accompanying O_2 formation and should thus correspond to K as defined here. According to the authors, however, a slower (100 ms) stabilization phase involving a further factor of more than 10 is also taking place. They ascribed this phase to O_2 release from the enzyme, in line with their earlier – and controversial – estimate for this reaction [98] (see Refs. [70,73–75,99] for studies supporting a fast release of O_2). Thus, according to this work, the value of K, including the stabilization accompanying O_2 release, should be $K \approx 650$; or only 65 if the 100 ms phase is ignored. Clearly, there is a huge discrepancy between these estimates and the much larger values obtained above from data concerning the oxidative part of the cycle (10^9–10^{15}). One may note that in the approach of Vos and colleagues, the value obtained for K relies crucially on the ascription of the weak electroluminescence signal detected at times ≥10 ms to the equilibrium concentration of Y_Z^{ox} formed by the reaction of S_0 with O_2. Any background signal (e.g. Y_Z^{ox} formed through equilibrium with Y_D^{ox}) or inaccuracy concerning the corrections made for the acceptor side relaxation or a "non-oscillating component" could cause serious under-estimation of K.

In the recent energy schemes elaborated by Siegbahn, based on density functional theory, the energy gap found for the S_4–S_0 reaction is 400 meV [19] or 750 meV [100] (the larger value being due to a re-

evaluation of the $P_{680}^{\bullet+}/P_{680}$ potential). This corresponds to a K in the 10^7–10^{12} range, thus in agreement with the high value suggested in the present work. It should be noticed, however, that in these energy schemes, the $P_{680}^{\bullet+}Y_ZM_3^+ \rightarrow P_{680}Y_Z^{ox}M_3^+$ reaction is significantly *uphill* by 170 meV [19] or 90 meV [100,101], at odds with experimental evidence showing that the oxidation of Y_Z by $P_{680}^{\bullet+}$ is thermodynamically favorable and precedes the proton release occurring in the $P_{680}Y_Z^{ox}M_3^+ \rightarrow P_{680}Y_Z^{ox}M_3 + H^+$ reaction [13,84]. While we do agree that the $P_{680}^{\bullet+}/P_{680}$ potential must be somewhat higher (by about 50 mV; Text S3 in Supplementary Material) in S_2 and S_3 due to the extra positive charge in the OEC, we think that this effect was overestimated (170–250 mV) by Siegbahn [100] in relation with the unfounded assumption that proton release electrostatically induced by $P_{680}^{\bullet+}$ precedes its reduction by Y_Z [100].

4.3. Entropy of product release and activation energy

Here, we revisit in the present context the considerations previously developed by Krishtalik concerning the energetics of the reaction $S_4 \rightarrow S_0 + O_2 + m\, H^+$ [102]. The release of the products (O_2 and H^+) implies an increase in translational and rotational entropy, which is an obligatory component of the ΔG_0. This component turns out to be quite significant, especially as the reference state adopted is not the usual 1 M convention, but 276 μM for O_2 and 10^{-7} M for protons. This has important consequences for the evolutionary tuning of the enzyme, which has to cope with this obligatory component of the driving force.

The energetics of product release from the active site can be tackled by considering a pathway where one first turns off the forces exerted by
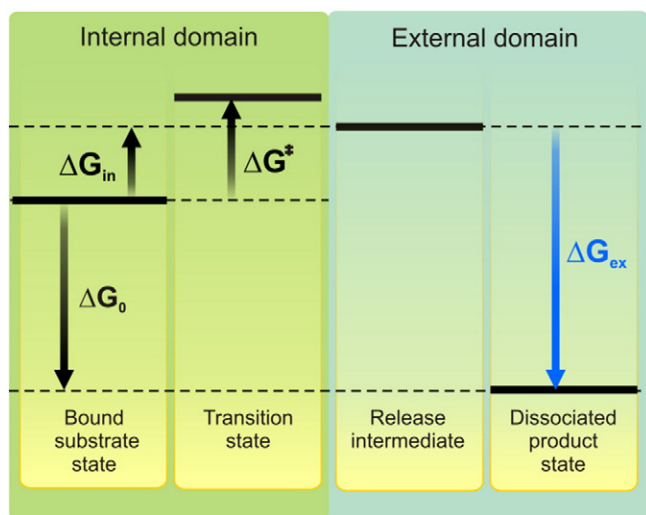
Fig. 7. A scheme showing the constraints to the energetic landscape implied by the release of the O_2 and H^+ products. The free energy drop from the release intermediate to the dissociated product state is essentially entropic (blue) and occurs in the external domain (ΔG_{ex}). The protein may tune the contribution ΔG_{in} related to the internal domain and reduce the overall ΔG_0 below ΔG_{ex}, as assumed here. However, the release intermediate is a fixed passage point, so that the activation free energy $\Delta G^{\ddagger}$ cannot be smaller than ΔG_{in}.

the protein on a given product in the active site before letting it diffuse into the external medium. In the intermediate state thus postulated (denoted henceforth as "release intermediate"), the product remains in the same region of space, but the protein is replaced by solvent. The solvation energy is thus assumed to have reached its relaxed value and the only thermodynamic force that remains is the change in translational and rotational entropy implied by the escape from the confined initial region of space. A simple reasoning related to the "cratic" (mixing) approach [103] is to consider that in the release intermediate the site is occupied by the product (with mole fraction 1), while in the final state it is occupied with frequencies $56/([O_2]_0 + 56)$ and $[O_2]_0 / ([O_2]_0 + 56)$ by water and by the O_2 product, respectively (the concentration of water is taken as 56 M). This predicts an entropy change of $R \times \ln(56 / [O_2]_0)$. For the release of O_2 at $[O_2]_0 = 273$ μM and $T = 298$ K, one obtains $T\Delta S = 314$ meV. For the release of one proton to the medium at pH = 7, this gives $T\Delta S = 516$ meV.

There has been a long-standing debate on the correctness of this and of alternative approaches (see e.g. Refs. [104–107]). Theoretical and experimental arguments supporting the cratic approach can be found in a recent study [107] and, conservatively, we retain here the cratic estimate for translational entropy, which results in smaller values than obtained from other approaches. And, also conservatively, we ignore (for lack of data) the rotational entropy contribution. Thus, the minimum entropic contribution to the ΔG_0 due to product release is $314 + 516 = 830$ meV. The protein has no grip on this "extra enzyme" contribution, that we denote ΔG_{ex} (see Fig. 7). The enzymatic domain of the reaction concerns what happens between the bound substrate state and the release intermediate and we denote by ΔG_{in} this "intra enzyme" contribution. Whereas ΔG_{ex} is purely entropic, one expects the entropic contribution to ΔG_{in} to be relatively small. In the overall $\Delta G_0 = \Delta G_{in} + \Delta G_{ex}$, the component accessible to evolutionary adaptation is obviously ΔG_{in}. The enzyme can lower the magnitude of the ΔG_0 below the 830 meV corresponding to ΔG_{ex} by setting an endergonic ΔG_{in}, as pictured in Fig. 7. There are some advantages in doing this: decreasing the ΔG_0 allows a lower midpoint potential for $P^{\bullet+}_{680}/P_{680}$, which will increase the reducing power at the electron acceptor side and will also render $P^{\bullet+}_{680}$ less reactive and hazardous to its environment. On the other hand, as illustrated in Fig. 7, one cannot decrease ΔG_0

by too much, because this would result in too large an activation energy for the reaction. Indeed, when ΔG_{in} is endergonic, the minimum activation energy is $|\Delta G_{in}|$, because the release intermediate is a fixed passage point.

We can estimate an upper bound for the activation free energy of the $P_{680}Y^{ox}_Z M_3 \rightarrow P_{680}Y_Z M_0 + O_2$ reaction which occurs with a ≈ 1 ms time constant $(1/k)$ by using Eyring's formula[1] (see [108] for caveats regarding the meaning of the pre-exponential factor): $k = k_B T / h \times \exp(-\Delta G^{\ddagger}/k_B T)$. In order to have $k \approx 1000$ s^{-1}, one should set $\Delta G^{\ddagger} = 580$ meV. If we adopt this value as the maximum depth of the "binding well" (see Fig. 7), i.e. $|\Delta G_{in}| \le 580$ meV, this implies $\Delta G_0 \ge 830-580 = 250$ meV, hence $K \ge 10^4$. Any additional "bump" locating the transition state above the energy level of the release intermediate, which is likely to happen, will result in a larger K. Thus again, this analysis shows that low values of the equilibrium constant such as estimated by Vos et al. [36] or by Clausen and Junge [52] are not plausible.

The activation enthalpy of the $S_4 \rightarrow S_0 + O_2$ reaction has been estimated in the 210–400 meV range by a number of studies (see Refs. [5,76,109,110]). Thus, the enthalpic depth of the binding well is at most ≈ 400 meV, which is in line with the above estimate $|\Delta G_{in}| \le 580$ meV. If the entropic contributions to ΔG_{in} are small, one would have $\Delta G_0 \ge 830-400 = 430$ meV, corresponding to $K \ge 10^7$. Another relevant piece of information arises from the photothermal beam deflection experiments reported in [111]. This work concluded that the $Y^{ox}_Z S_3 \rightarrow Y_Z S_0 + O_2$ reaction is slightly exothermic (i.e. $\Delta H_0 \approx -210$ meV, but a value of 0 was within experimental accuracy). This would locate the bound state enthalpy level close to or above that of the release intermediate, implying that the activation enthalpy of 300–400 meV is essentially due to a bump locating the transition state above the release state. In this case, if entropic contributions to the ΔG_{in} were negligible, one would have $\Delta G_0 \ge 830$ meV and $K \ge 10^{14}$, which is close to the upper limit (10^{15}) estimated in the previous section.

5. Conclusions

The experimental approaches and the theoretical analyses reported in this paper point to a much larger driving force for the $S_4 \rightarrow S_0$ reaction than generally believed. Using a new experimental approach (OWIE), which offers a very high sensitivity, we obtained a negative result that pushes the lower bound for K above 1.0×10^7. This is close to the lower bound that we obtained independently by using the available information on the energetics of the S-state transitions ($10^9 \le K \le 10^{15}$). Finally, following Krishtalik [102], we pointed to the importance of the entropic contribution to the overall driving force due to the release of products. Photosystem II can lower the ΔG_0 to some extent, but this occurs at the expense of an increased activation barrier. Hence, for ensuring kinetic efficiency, K must be $\ge 10^4$. This lower bound must still be significantly raised if one takes into account current estimates for the activation enthalpy and the finding of a slightly exothermic overall reaction.

Transparency document

The Transparency document associated with this article can be found, in online version.

---

[1] The purpose here is essentially to obtain a rough order of magnitude for the maximum activation energy compatible with a 1 ms reaction. The Eyring (transition state) theory may not be fully suitable here, since e.g. the reaction involves electron transfer steps which are better handled by the Marcus theory.

Acknowledgments

Appendix A. Supplementary data

Supplementary data to this article can be found online at http://dx.doi.org/10.1016/j.bbabio.2015.09.011.

References

[1] T. Faunce, S. Styring, M.R. Wasielewski, G.W. Brudvig, A.W. Rutherford, J. Messinger, A.F. Lee, C.L. Hill, H. de Groot, M. Fontecave, D.R. MacFarlane, B. Hankamer, D.G. Nocera, D.M. Tiede, H. Dau, W. Hillier, L.Z. Wang, R. Amal, Artificial photosynthesis as a frontier technology for energy sustainability, Energy Environ. Sci. 6 (2013) 1074–1076.

[2] A.R. Holzwarth, M.G. Müller, M. Reus, M. Nowaczyk, J. Sander, M. Rögner, Kinetics and mechanism of electron transfer in intact photosystem II and in the isolated reaction center: pheophytin is the primary electron acceptor, Proc. Natl. Acad. Sci. U. S. A. 103 (2006) 6895–6900.

[3] G. Renger, The light reactions of photosynthesis, Curr. Sci. 98 (2010) 1305–1319.

[4] G.D. Scholes, G.R. Fleming, A. Olaya-Castro, R. van Grondelle, Lessons from nature about solar light harvesting, Nat. Chem. 3 (2011) 763–774.

[5] G. Renger, Mechanism of light induced water splitting in photosystem II of oxygen evolving photosynthetic organisms, Biochim. Biophys. Acta 1817 (2012) 1164–1176.

[6] A.W. Rutherford, A. Osyczka, F. Rappaport, Back-reactions, short-circuits, leaks and other energy wasteful reactions in biological electron transfer: redox tuning to survive life in O_2, FEBS Lett. 586 (2012) 603–616.

[7] T. Cardona, A. Sedoud, N. Cox, A.W. Rutherford, Charge separation in photosystem II: a comparative and evolutionary overview, Biochim. Biophys. Acta 1817 (2012) 26–43.

[8] D.J. Vinyard, G.M. Ananyev, G.C. Dismukes, Photosystem II: the reaction center of oxygenic photosynthesis, Annu. Rev. Biochem. 82 (2013) 577–606.

[9] E. Romero, R. Augulis, V.I. Novoderezhkin, M. Ferretti, J. Thieme, D. Zigmantas, R. van Grondelle, Quantum coherence in photosynthesis for efficient solar-energy conversion, Nat. Phys. 10 (2014) 677–683.

[10] N. Nelson, W. Junge, Structure and energy transfer in photosystems of oxygenic photosynthesis, Annu. Rev. Biochem. 84 (2015) http://dx.doi.org/10.1146/annurev-biochem-092914-041942.

[11] F. Rappaport, M. Guergova-Kuras, P.J. Nixon, B.A. Diner, J. Lavergne, Kinetics and pathways of charge recombination in photosystem II, Biochemistry 41 (2002) 8518–8527.

[12] M. Grabolle, H. Dau, Energetics of primary and secondary electron transfer in photosystem II membrane particles of spinach revisited on basis of recombination-fluorescence measurements, Biochim. Biophys. Acta 1708 (2005) 209–218.

[13] F. Rappaport, B.A. Diner, Primary photochemistry and energetics leading to the oxidation of the $(Mn)_4Ca$ cluster and to the evolution of molecular oxygen in photosystem II, Coord. Chem. Rev. 252 (2008) 259–272.

[14] T. Shibamoto, Y. Kato, M. Sugiura, T. Watanabe, Redox potential of the primary plastoquinone electron acceptor Q_A in photosystem II from *Thermosynechococcus elongatus* determined by spectroelectrochemistry, Biochemistry 48 (2009) 10682–10684.

[15] A.-M.A. Hays, I.R. Vassiliev, J.H. Golbeck, R.J. Debus, Role of D1-His190 in proton-coupled electron transfer reactions in photosystem II: a chemical complementation study, Biochemistry 37 (1998) 11352–11365.

[16] F. Rappaport, A. Boussac, D.A. Force, J. Peloquin, M. Brynda, M. Sugiura, S. Un, R.D. Britt, B.A. Diner, Probing the coupling between proton and electron transfer in photosystem II core complexes containing a 3-fluorotyrosine, J. Am. Chem. Soc. 131 (2009) 4425–4433.

[17] J. Yano, J. Kern, K. Sauer, M.J. Latimer, Y. Pushkar, J. Biesiadka, B. Loll, W. Saenger, J. Messinger, A. Zouni, V.K. Yachandra, Where water is oxidized to dioxygen: structure of the photosynthetic Mn4Ca cluster, Science 314 (2006) 821–825.

[18] H. Dau, A. Grundmeier, P. Loja, M. Haumann, On the structure of the manganese complex of photosystem II: extended-range EXAFS data and specific atomic-resolution models for four S-states, Philos. Trans. R. Soc. Lond. B 363 (2008) 1237–1243.

[19] P.E.M. Siegbahn, Structures and energetics for O_2 formation in photosystem II, Acc. Chem. Res. 42 (2009) 1871–1880.

[20] Y. Umena, K. Kawakami, J.R. Shen, N. Kamiya, Crystal structure of oxygen-evolving photosystem II at a resolution of 1.9 Å, Nature 473 (2011) 55–61.

[21] M. Suga, F. Akita, K. Hirata, G. Ueno, H. Murakami, Y. Nakajima, T. Shimizu, K. Yamashita, M. Yamamoto, H. Ago, J.R. Shen, Native structure of photosystem II at 1.95 angstrom resolution viewed by femtosecond X-ray pulses, Nature 517 (2015) 99–103.

[22] A. Boussac, N. Ishida, M. Sugiura, F. Rappaport, Probing the role of chloride in photosystem II from *Thermosynechococcus elongatus* by exchanging chloride for iodide, Biochim. Biophys. Acta 1817 (2012) 802–810.

[23] E.M. Sproviero, K. Shinopoulos, J.A. Gascon, J.P. McEvoy, G.W. Brudvig, V.S. Batista, QM/MM computational studies of substrate water binding to the oxygen-evolving centre of photosystem II, Philos. Trans. R. Soc. Lond. B 363 (2008) 1149–1156.

[24] H. Dau, C. Limberg, T. Reier, M. Risch, S. Roggan, P. Strasser, The mechanism of water oxidation: from electrolysis via homogeneous to biological catalysis, ChemCatChem 2 (2010) 724–761.

[25] I. Zaharieva, J.M. Wichmann, H. Dau, Thermodynamic limitations of photosynthetic water oxidation at high proton concentrations, J. Biol. Chem. 286 (2011) 18222–18228.

[26] H. Dau, I. Zaharieva, M. Haumann, Recent developments in research on water oxidation by photosystem II, Curr. Opin. Chem. Biol. 16 (2012) 3–10.

[27] J. Messinger, T. Noguchi, J. Yano, Photosynthetic O_2 evolution, in: T.J. Wydrzynski, W. Hillier (Eds.) Molecular Solar Fuels RSC, London, 2012, pp. 163–207.

[28] N. Cox, D.A. Pantazis, F. Neese, W. Lubitz, Biological water oxidation, Acc. Chem. Res. 46 (2013) 1588–1596.

[29] N. Cox, J. Messinger, Reflections on substrate water and dioxygen formation, Biochim. Biophys. Acta 1827 (2013) 1020–1030.

[30] N. Cox, M. Retegan, F. Neese, D.A. Pantazis, A. Boussac, W. Lubitz, Electronic structure of the oxygen-evolving complex in photosystem II prior to O–O bond formation, Science 345 (2014) 804–808.

[31] J.-R. Shen, The structure of photosystem II and the mechanism of water oxidation in photosynthesis, Annu. Rev. Plant Biol. 66 (2015), http://dx.doi.org/10.1146/annurev-arplant-050312-120129.

[32] M. Broser, A. Gabdulkhakov, J. Kern, A. Guskov, F. Muh, W. Saenger, A. Zouni, Crystal structure of monomeric photosystem II from *Thermosynechococcus elongatus* at 3.6-Angstrom resolution, J. Biol. Chem. 285 (2010) 26255–26262.

[33] V. Krewald, M. Retegan, N. Cox, J. Messinger, W. Lubitz, S. DeBeer, F. Neese, D.A. Pantazis, Metal oxidation states in biological water splitting, Chem. Sci. 6 (2015) 1676–1695.

[34] B. Kok, B. Forbush, M. McGloin, Cooperation of charges in photosynthetic O_2 evolution, Photochem. Photobiol. 11 (1970) 457–476.

[35] P. Joliot, B. Kok, Oxygen evolution in photosynthesis, in: Govindjee (Ed.), Bioenergetics of Photosynthesis, Academic Press, New York, NY 1975, pp. 387–412.

[36] M.H. Vos, H.J. van Gorkom, P.J. van Leeuwen, An electroluminescence study of stabilization reactions in the oxygen evolving complex of photosystem II, Biochim. Biophys. Acta 1056 (1991) 27–39.

[37] J. Messinger, G. Renger, Photosynthetic water-splitting, in: G. Renger (Ed.), Primary Processes of Photosynthesis — Part 2: Basic Principles and Apparatus, The Royal Society of Chemistry, Cambridge, UK 2008, pp. 291–349.

[38] F. Rappaport, J. Lavergne, Proton release during successive oxidation steps of the photosynthetic water oxidation process — stoichiometries and pH-dependence, Biochemistry 30 (1991) 10004–10012.

[39] J. Lavergne, W. Junge, Proton release during the redox cycle of the water oxidase, Photosynth. Res. 38 (1993) 279–296.

[40] E. Schlodder, H.T. Witt, Stoichiometry of proton release from the catalytic center in photosynthetic water oxidation, J. Biol. Chem. 274 (1999) 30387–30392.

[41] B.R. Velthuys, Akoyunoglou, Spectroscopic studies of the S state transitions of photosystem II and the interactions of its charged donor chain with lipid-soluble anions, Proceedings of the Vth International Congress on Photosynthesis, Rehovot, Balaban 1981, pp. 75–85.

[42] Ö. Saygin, H.T. Witt, Evidence for the electrochromic identification of the change of charges in the 4 oxidation steps of the photoinduced water cleavage in photosynthesis, FEBS Lett. 187 (1985) 224–226.

[43] A. Klauss, M. Haumann, H. Dau, Alternating electron and proton transfer steps in photosynthetic water oxidation, Proc. Natl. Acad. Sci. U. S. A. 109 (2012) 16035–16040.

[44] J. Messinger, M. Badger, T. Wydrzynski, Detection of *one* slowly exchanging substrate water molecule in the S_3 state of photosystem II, Proc. Natl. Acad. Sci. U. S. A. 92 (1995) 3209–3213.

[45] H. Nilsson, F. Rappaport, A. Boussac, J. Messinger, Substrate-water exchange in photosystem II is arrested prior to dioxygen formation, Nat. Commun. 5 (2014) 4305.

[46] L. Rapatskiy, N. Cox, A. Savitsky, W.M. Ames, J. Sander, M.M. Nowaczyk, M. Rögner, A. Boussac, F. Neese, J. Messinger, W. Lubitz, Detection of the water-binding sites of the oxygen-evolving complex of photosystem II using W-band ^{17}O electron–electron double resonance–detected NMR spectroscopy, J. Am. Chem. Soc. 134 (2012) 16619–16634.

[47] F.H.M. Koua, Y. Umena, K. Kawakami, J.R. Shen, Structure of Sr-substituted photosystem II at 2.1 Å resolution and its implications in the mechanism of water oxidation, Proc. Natl. Acad. Sci. U. S. A. 110 (2013) 3889–3894.

[48] M.P. Navarro, W.M. Ames, H. Nilsson, T. Lohmiller, D.A. Pantazis, L. Rapatskiy, M.M. Nowaczyk, F. Neese, A. Boussac, J. Messinger, W. Lubitz, N. Cox, Ammonia binding to the oxygen-evolving complex of photosystem II identifies the solvent–exchangeable oxygen bridge (μ-oxo) of the manganese tetramer, Proc. Natl. Acad. Sci. U. S. A. 110 (2013) 15561–15566.

[49] H. Nilsson, T. Krupnik, J. Kargul, J. Messinger, Substrate water exchange in photosystem II core complexes of the extremophilic red alga *Cyanidioschyzon merolae*, Biochim. Biophys. Acta 1837 (2014) 1257–1262.

[50] H. Suzuki, M. Sugiura, T. Noguchi, Monitoring water reactions during the S-state cycle of the photosynthetic water-oxidizing center: detection of the DOD bending vibrations by means of Fourier transform infrared spectroscopy, Biochemistry 47 (2008) 11024–11030.

[51] T. Noguchi, FTIR detection of water reactions in the oxygen-evolving centre of photosystem II, Philos. Trans. R. Soc. Lond. B 363 (2008) 1189–1194.

[52] J. Clausen, W. Junge, Detection of an intermediate of photosynthetic water oxidation, Nature 430 (2004) 480–483.

[53] M. Haumann, A. Grundmeier, I. Zaharieva, H. Dau, Photosynthetic water oxidation at elevated dioxygen partial pressure monitored by time-resolved X-ray absorption measurements, Proc. Natl. Acad. Sci. U. S. A. 105 (2008) 17384–17389.

[54] D.R.J. Kolling, T.S. Brown, G. Ananyev, G.C. Dismukes, Photosynthetic oxygen evolution is not reversed at high oxygen pressures: mechanistic consequences for the water-oxidizing complex, Biochemistry 48 (2009) 1381–1389.

[55] D. Shevela, K. Beckmann, J. Clausen, W. Junge, J. Messinger, Membrane-inlet mass spectrometry reveals a high driving force for oxygen production by photosystem II, Proc. Natl. Acad. Sci. U. S. A. 108 (2011) 3602–3607.

[56] M. Sugiura, F. Rappaport, K. Brettel, T. Noguchi, A.W. Rutherford, A. Boussac, Site-directed mutagenesis of the *Thermosynechococcus elongatus* photosystem II: the O₂-evolving enzyme lacking the redox-active tyrosine D, Biochemistry 43 (2004) 13549–13563.

[57] R. Sander, Compilation of Henry's law constants (version 4.0) for water as solvent, Atmos. Chem. Phys. 15 (2015) 4399–4981.

[58] CODATA value:molar gas constant, NIST, 2015. http://physics.nist.gov/cgi-bin/cuu/Value?r.

[59] M. Knox, P.D. Quay, D. Wilbur, Kinetic isotopic fractionation during air–water gas transfer of O₂, N₂, CH₄, and H₂, J. Geophys. Res.-Oceans 97 (1992) 20335–20343.

[60] L. Konermann, J. Messinger, W. Hillier, Mass spectrometry based methods for studying kinetics and dynamics in biological systems, in: T.J. Aartsma, J. Matysik (Eds.), Biophysical Techniques in Photosynthesis (Volume II), Springer, Dordrecht 2008, pp. 167–190.

[61] K. Beckmann, J. Messinger, M.R. Badger, T. Wydrzynski, W. Hillier, On-line mass spectrometry: membrane inlet sampling, Photosynth. Res. 102 (2009) 511–522.

[62] D. Shevela, J. Messinger, Studying the oxidation of water to molecular oxygen in photosynthetic and artificial systems by time-resolved membrane-inlet mass spectrometry, Front. Plant Sci. 4 (2013).

[63] G. Renger, B. Bouges-Bocquet, R. Delosme, Studies on a dry agent-induced mechanism of discharge of holes trapped in photosynthetic watersplitting enzyme system-Y, Biochim. Biophys. Acta 292 (1973) 796–807.

[64] B. Hanssum, G. Renger, W. Weiss, Studies on the reaction-mechanism of tetraphenylboron at the photosystem II donor side in isolated spinach-chloroplasts, Biochim. Biophys. Acta 808 (1985) 243–251.

[65] J. Lavergne, Improved UV–visible spectra of S-state transitions in the photosynthetic oxygen evolving system, Biochim. Biophys. Acta 1060 (1991) 175–188.

[66] J. Messinger, J.H. Robblee, W.O. Yu, K. Sauer, V.K. Yachandra, M.P. Klein, The S₀ state of the oxygen evolving complex in photosystem II is paramagnetic: detection of an EPR multiline signal, J. Am. Chem. Soc. 119 (1997) 11349–11350.

[67] K.A. Åhrling, S. Peterson, S. Styring, An oscillating manganese electron paramagnetic resonance signal from the S₀ state of the oxygen evolving complex in photosystem II, Biochemistry 36 (1997) 13148–13152.

[68] W. Hillier, J. Messinger, T. Wydrzynski, Kinetic determination of the fast exchanging substrate water molecule in the S₃ state of photosystem II, Biochemistry 37 (1998) 16908–16914.

[69] M. Sugiura, F. Rappaport, W. Hillier, P. Dorlet, Y. Ohno, H. Hayashi, A. Boussac, Evidence that D1-His332 in photosystem II from *Thermosynechococcus elongatus* interacts with the S₃-state and not with the S₂-state, Biochemistry 48 (2009) 7856–7866.

[70] P. Joliot, M. Hofnung, R. Chabaud, Etude de l'emission d'oxygene par des algues soumises a un eclairement module sinusoidalement, J. Chim. Phys. 63 (1966) 1423–1441.

[71] P.A. Jursinic, R.J. Dennenberg, Oxygen release time in leaf disks and thylakoids of peas and photosystem II membrane fragments of spinach, Biochim. Biophys. Acta 1020 (1990) 195–206.

[72] K. Strzalka, T. Walczak, T. Sarna, H.M. Swartz, Measurement of time-resolved oxygen concentration changes in photosynthetic systems by nitroxide-based EPR oximetry, Arch. Biochem. Biophys. 281 (1990) 312–318.

[73] J. Lavergne, Detection of photosynthetic oxygen through mitochondrial absorption changes in algal cells, in: M. Baltscheffsky (Ed.) Current Research in Photosynthesis, 1–4, Kluwer Academic Publ, Dordrecht 1990, pp. A893–A896.

[74] P.C. Meunier, R. Popovic, The time for oxygen release in photosynthesis: reconciliation of flash polarography with other measurement techniques, Photosynth. Res. 28 (1991) 33–39.

[75] J. Lavorel, Determination of photosynthetic oxygen release time by amperometry, Biochim. Biophys. Acta 1101 (1992) 33–40.

[76] J. Clausen, R.J. Debus, W. Junge, Time-resolved oxygen production by PSII: chasing chemical intermediates, Biochim. Biophys. Acta 1655 (2004) 184–194.

[77] L.Y. Yeung, J.L. Ash, E.D. Young, Biological signatures in clumped isotopes of O₂, Science 348 (2015) 431–434.

[78] S. Isgandarova, G. Renger, J. Messinger, Functional differences of photosystem II from *Synechococcus elongatus* and spinach characterized by flash induced oxygen evolution patterns, Biochemistry 42 (2003) 8929–8938.

[79] A. Boussac, F. Rappaport, P. Carrier, J.M. Verbavatz, R. Gobin, D. Kirilovsky, A.W. Rutherford, M. Sugiura, Biosynthetic Ca^{2+}/Sr^{2+} exchange in the photosystem II oxygen-evolving enzyme of *Thermosynechococcus elongatus*, J. Biol. Chem. 279 (2004) 22809–22819.

[80] K. Brettel, E. Schlodder, H.T. Witt, Nanosecond reduction kinetics of photooxidised chlorophyll a_II (P680) in single flashes as a probe for the electron pathway, H⁺ release and charge accumulation in the O₂ evolving complex, Biochim. Biophys. Acta 766 (1984) 403–415.

[81] M.J. Schilstra, F. Rappaport, J.H.A. Nugent, C.J. Barnett, D.R. Klug, Proton/hydrogen transfer affects the S-state dependent microsecond phases of P680⁺ reduction during water splitting, Biochemistry 37 (1998) 3974–3981.

[82] G. Christen, G. Renger, The role of hydrogen bonds for the multiphasic P680⁺· reduction by Y_Z in photosystem II with intact oxygen evolution capacity. Analysis of kinetic H/D isotope exchange effects, Biochemistry 38 (1999) 2068–2077.

[83] F. Rappaport, M. Blanchard-Desce, J. Lavergne, Kinetics of electron-transfer and electrochromic change during the redox transitions of the photosynthetic oxygen-evolving complex, Biochim. Biophys. Acta 1184 (1994) 178–192.

[84] M. Haumann, P. Liebisch, C. Müller, M. Barra, M. Grabolle, H. Dau, Photosynthetic O₂ formation tracked by time-resolved X-ray experiments, Science 310 (2005) 1019–1021.

[85] N. Ishida, M. Sugiura, F. Rappaport, T.L. Lai, A.W. Rutherford, A. Boussac, Biosynthetic exchange of bromide for chloride and strontium for calcium in the photosystem II oxygen-evolving enzymes, J. Biol. Chem. 283 (2008) 13330–13340.

[86] L. Gerencser, H. Dau, Water oxidation by photosystem II: H₂O–D₂O exchange and the influence of pH support formation of an intermediate by removal of a proton before dioxygen creation, Biochemistry 49 (2010) 10098–10106.

[87] T. Noguchi, H. Suzuki, M. Tsuno, M. Sugiura, C. Kato, Time-resolved infrared detection of the proton and protein dynamics during photosynthetic oxygen evolution, Biochemistry 51 (2012) 3205–3214.

[88] T. Noguchi, Fourier transform infrared difference and time-resolved infrared detection of the electron and proton transfer dynamics in photosynthetic water oxidation, Biochim. Biophys. Acta 1847 (2015) 35–45.

[89] G.T. Babcock, R.E. Blankenship, K. Sauer, Reaction kinetics for positive charge accumulation on the water side of chloroplast photosystem II, FEBS Lett. 61 (1976) 286–289.

[90] P.J. van Leeuwen, C. Heimann, H.J. van Gorkom, Absorbance difference spectra of the S-state transitions in photosystem II core particles, Photosynth. Res. 38 (1993) 323–330.

[91] M. Haumann, O. Bögershausen, D. Cherepanov, R. Ahlbrink, W. Junge, Photosynthetic oxygen evolution: H/D isotope effects and the coupling between electron and proton transfer during the redox reactions at the oxidizing side of photosystem II, Photosynth. Res. 51 (1997) 193–208.

[92] M.R. Razeghifard, R.J. Pace, EPR kinetic studies of oxygen release in thylakoids in PSII membranes: a kinetic intermediate in the S₃ to S₀ transition, Biochemistry 38 (1999) 1252–1257.

[93] P.E.M. Siegbahn, Substrate water exchange for the oxygen evolving complex in PSII in the S₁, S₂, and S₃ states, J. Am. Chem. Soc. 135 (2013) 9442–9449.

[94] A.W. Rutherford, G. Renger, H. Koike, Y. Inoue, Thermo-luminescence as a probe of photosystem II — the redox and protonation states of the secondary acceptor quinone and the O₂-evolving enzyme, Biochim. Biophys. Acta 767 (1984) 548–556.

[95] Y. Inoue, Photosynthetic thermoluminescence as a simple probe of photosystem II electron transport, in: J. Amesz, A.J. Hoff (Eds.), Biophysical Thechniques in Photosynthesis, Kluwer Academic Publishers, Dordrecht 1996, pp. 93–107.

[96] F. Rappaport, J. Lavergne, Thermoluminescence: theory, Photosynth. Res. 101 (2009) 205–216.

[97] I. Vass, S. Styring, pH dependent charge equilibria between tyrosine D and the S states in photosystem II. Estimation of relative midpoint potentials, Biochemistry 30 (1991) 830–839.

[98] J.J. Plijter, S.E. Aalbers, J.P.F. Barends, M.H. Vos, H.J. van Gorkom, Oxygen release may limit the rate of photosynthetic electron-transport — the use of a weakly polarized oxygen cathode, Biochim. Biophys. Acta 935 (1988) 299–311.

[99] M. Hundelt, A.-M.A. Hays, R.J. Debus, W. Junge, Oxygenic photosystem II: the mutation D1-D61N in *Synechocystis* sp. PCC 6803 retards S-state transitions without affecting electron transfer from Y_Z to P680⁺, Biochemistry 37 (1998) 14450–14456.

[100] P.E.M. Siegbahn, Water oxidation mechanism in photosystem II, including oxidations, proton release pathways, O–O bond formation and O₂ release, Biochim. Biophys. Acta 1827 (2013) 1003–1019.

[101] P.E.M. Siegbahn, Mechanisms for proton release during water oxidation in the S₂ to S₃ and S₃ to S₄ transitions in photosystem II, Phys. Chem. Chem. Phys. 14 (2012) 4849–4856.

[102] L.I. Krishtalik, Energetics of multielectron reactions. Photosynthetic oxygen evolution, Biochim. Biophys. Acta 849 (1986) 162–171.

[103] R. Gurney, Ionic Processes in Solution, McGraw-Hill, New York, 1953.

[104] K.P. Murphy, D. Xie, K.S. Thompson, L.M. Amzel, E. Freire, Entropy in biological binding processes — estimation of translational entropy loss, Proteins 18 (1994) 63–67.

[105] X. Siebert, L.M. Amzel, Loss of translational entropy in molecular associations, Proteins 54 (2004) 104–115.

[106] H.X. Zhou, M.K. Gilson, Theory of free energy and entropy in noncovalent binding, Chem. Rev. 109 (2009) 4092–4107.

[107] S.J. Irudayam, R.H. Henchman, Entropic cost of protein–ligand binding and its dependence on the entropy in solution, J. Phys. Chem. B 113 (2009) 5871–5884.

[108] H.X. Zhou, Rate theories for biologists, Q. Rev. Biophys. 43 (2010) 219–293.

[109] G. Renger, B. Hanssum, Studies on the reaction coordinates of the water oxidase in PSII membrane-fragments from spinach, FEBS Lett. 299 (1992) 28–32.

[110] J. Buchta, M. Grabolle, H. Dau, Photosynthetic dioxygen formation studied by time-resolved delayed fluorescence measurements — method, rationale, and results on the activation energy of dioxygen formation, Biochim. Biophys. Acta 1767 (2007) 565–574.

[111] R. Krivanek, H. Dau, M. Haumann, Enthalpy changes during photosynthetic water oxidation tracked by time-resolved calorimetry using a photothermal beam deflection technique, Biophys. J. 94 (2008) 1890–1903.